Molecular Biology of the Cell
Vol. 10, 1665–1683, May 1999

Ras Family GTPases Control Growth of Astrocyte Processes

Daniel Kalman,*† Stephen N. Gomperts,‡ Stephen Hardy,§ Marina Kitamura,§ and J. Michael Bishop*

*Department of Microbiology and Immunology, G. W. Hooper Foundation Laboratories, and ‡Neuroscience Graduate Program, University of California at San Francisco, San Francisco, California 94143; and §Cell Genesys Inc., Foster City, California 94404

Submitted January 5, 1999; Accepted February 26, 1999
Monitoring Editor: Martin Raff

Astrocytes in neuron-free cultures typically lack processes, although they are highly process-bearing in vivo. We show that basic fibroblast growth factor (bFGF) induces cultured astrocytes to grow processes and that Ras family GTPases mediate these morphological changes. Activated alleles of *rac1* and *rhoA* blocked and reversed bFGF effects when introduced into astrocytes in dissociated culture and in brain slices using recombinant adenoviruses. By contrast, dominant negative (DN) alleles of both GTPases mimicked bFGF effects. A DN allele of Ha-*ras* blocked bFGF effects but not those of Rac1-DN or RhoA-DN. Our results show that bFGF acting through c-Ha-Ras inhibits endogenous Rac1 and RhoA GTPases thereby triggering astrocyte process growth, and they provide evidence for the regulation of this cascade in vivo by a yet undetermined neuron-derived factor.

INTRODUCTION

In the nervous system, astrocytes are highly process-bearing cells. Their processes serve as tracts for migrating neuroblasts (Cameron and Rakic, 1991), and contact nodes of Ranvier and ensheathe synapses where they buffer potassium ions and neurotransmitters (Ffrench-Constant *et al.*, 1986; Mennerick and Zorumski, 1994; Hansson and Ronnback, 1995; Sontheimer, 1995; Mennerick *et al.*, 1996). When astrocytes are removed from the brain into cell culture in the absence of neurons, they fail to extend their processes and instead divide and grow as a flat fibroblast-like contact-inhibited monolayer (Hatten, 1985). Exposure of cultured astrocytes to live neurons induces them to form processes and to assume a morphology reminiscent of that in adult brain (Hatten, 1985; Gasser and Hatten, 1990). These observations suggest that a neuron-derived factor normally sculpts the adult morphology of astrocytes in vivo.

Although much is currently known about the signals that guide and speed the growth of neuronal processes, less is known about the mechanisms that induce process formation in astrocytes and neurons. Recent progress, however, has implicated the Ras family of GTPases, which includes c-Ha-Ras, Cdc42, Rac1, and RhoA, in controlling membrane and cytoskeletal reorganization in various cell types (reviewed in Van Aelst and D'Souza-Schorey, 1997). In non-neural cells, Cdc42 appears to cause filopodial extensions (Kozma *et al.*, 1995; Nobes and Hall, 1995), Rac1 produces lamellipodia and membrane ruffling (Ridley *et al.*, 1992), and RhoA produces actin bundles and focal adhesions (Ridley and Hall, 1992). Such membrane structures and rearrangements are also found in the growth cones of processes in both neurons (reviewed in Cramer, 1997) and astrocytes (Mason *et al.*, 1988; Kalman and Gomperts, unpublished observations). In neurons, Cdc42, Rac1, and RhoA have been implicated in process growth and growth cone dynamics (Kozma *et al.*, 1997; Leeuwen *et al.*, 1997; Threadgill *et al.*, 1997; Daniels *et al.*, 1998). For example, Cdc42 and/or Rac1 act to promote growth cone extension, in opposition to the effects of RhoA (Kozma *et al.*, 1997; Leeuwen *et al.*, 1997; however, see Threadgill *et al.*, 1997). In astrocytes, RhoA has been implicated, albeit indirectly, in a membrane retraction event called "cavitation," which is produced by the addition of membrane-permeable

† Corresponding author. E-mail address: kalman@cgl.ucsf.edu.

analogues of cAMP (Koyama and Baba, 1996; see also Goldman and Chiu, 1984; Goldman and Abramson, 1990; Baorto *et al.*, 1992).

Importantly, growth factors and other signaling molecules regulate small GTPase activity. For example, PDGF and Ha-Ras can activate Rac1-dependent events in fibroblasts (Ridley and Hall, 1992), endothelins activate RhoA in astrocytes (Koyama and Baba, 1996), and Rac1 has been implicated in nerve growth factor (NGF)[1]-induced process growth in PC12 cells (Daniels *et al.*, 1998). In addition, Cdc42, Rac1, and RhoA appear to be coupled in some but not all cell types (Nobes and Hall, 1995; Kozma *et al.*, 1997; Leeuwen *et al.*, 1997). In Swiss 3T3 fibroblasts, for example, Cdc42 can induce transient filopodial extensions followed by Rac1-dependent lamellipodia (Kozma *et al.*, 1995; Nobes and Hall, 1995). Likewise, Rac1 appears capable of inducing not just lamellipodia but also actin bundles, an event blocked by dominant inhibitory RhoA alleles (Ridley and Hall, 1992; Peppelenbosch *et al.*, 1995).

The observation that filopodia and lamellipodia occur along and at the tips of developing astrocyte processes (Mason *et al.*, 1988; Kalman and Gomperts, unpublished observations), and the reported role of RhoA in antagonizing process growth both in neurons and in astrocytes (Koyama and Baba, 1996; Kozma *et al.*, 1997; Leeuwen *et al.*, 1997), has led us to examine the role of small GTPases of the Ras superfamily in initiation, growth, and maintenance of processes of neonatal rat hippocampal astrocytes. We have identified basic fibroblast growth factor (bFGF) as a potent inducer of process growth and membrane retraction in cultured astrocytes (see also Perraud *et al.*, 1988). By expressing dominant inhibitory or constitutively active forms of the Ras family members, we have defined a signal transduction cascade in which bFGF, acting via Ha-Ras, inhibits Rac1 and RhoA. This cascade differs substantially from that described in cultured neurons (Kozma *et al.*, 1997; Leeuwen *et al.*, 1997; see also Threadgill *et al.*, 1997). Our results suggest that culturing of astrocytes upregulates the activity of Rac1 and RhoA, thereby causing loss of processes and cell spreading. bFGF causes membrane retraction by inhibiting Rac1 and RhoA activity and driving consequent actin reorganization in the cell soma. FGF also causes process growth that depends on this inhibition, but in addition requires extension of actin at the cell periphery into the growing processes. Rac1 and RhoA alleles act identically on astrocytes in organotypic hippocampal slice cultures. Our results raise the possibility that the GTPase cascade initiated by bFGF may play an important role in vivo in regulating astrocyte morphology, although it is not yet clear which growth factor triggers the cascade.

[1] Abbreviations used: Ad, adenovirus; bFGF, basic fibroblast growth factor; CMV, cytomegalovirus; dbcAMP, dibutyryl cyclic AMP; DN, dominant negative; GFAP, glial fibrillary acidic protein; GFP, Green Fluorescent Protein; LIF, leukemia inhibitory factor; NGF, nerve growth factor; PAK, p21-activated kinase.

MATERIALS AND METHODS

Culturing Primary Hippocampal Astrocytes and Organotypic Hippocampal Slices

Hippocampi of postnatal day (P0) Sprague Dawley rat pups were removed, and the dentate gyri were grossly dissected. Cells derived from the remaining tissue were isolated as described by Lester *et al.* (1989) and plated onto glass coverslips previously coated with collagen (60 μg/ml; Invitrogen, San Diego, CA) and poly-D-lysine (200 μg/ml; Sigma, St. Louis, MO). The cells were grown in DMEM supplemented with 10% FCS ("complete" media). Half of the growth media was exchanged at weekly intervals. The microdissection procedure yielded cultures that contained predominantly astrocytes (>99%) and a small number of neurons (<1%) as assessed by staining with antibodies recognizing the neuronal markers GAP-43 and MAP-2, or the astrocyte marker glial fibrillary acidic protein (GFAP) (Bignami *et al.*, 1972). We found no evidence for fibroblasts in the culture (i.e., flat, contact-inhibited cells that were not GFAP immunoreactive). For some experiments, media was supplemented with bFGF (Life Technologies-BRL, Gaithersburg, MD) at 0.01–1 ng/ml, EGF (Life Technologies-BRL) at 50 ng/ml, PDGF-AA (Life Technologies-BRL) at 50 ng/ml, TGF-β (a gift of R. Derynk, UCSF) at 50 ng/ml, NGF (Boehringer Mannheim, Indianapolis, IN) at 100 ng/ml, or leukemia inhibitory factor (a gift of S. Kogan, UCSF) at 50 ng/ml. Growth factors in the media were replenished every 2 d. Cultures were used within the first 3 wk after plating, because cells cultured for longer than that underwent spontaneous morphological changes. For organotypic cultures, 400-μm-thick slices of hippocampus from P0 rats were placed on top of millicell filter membranes (Millipore, Bedford, MA), and floated in 35-mm tissue culture dishes containing 1 ml of MEM supplemented with HBSS (25 mM), glutamine (2 mM), and 25% heat-inactivated horse serum (Stoppini *et al.*, 1991).

Generation of Recombinant Adenoviruses

For virus construction, cDNA sequences encoding the Rac1 alleles (V12, activated; V12/N17 or N17, dominant negatives) (Ridley and Hall, 1992; Ridley *et al.*, 1992), or RhoA alleles (V14 or L63, activated; N19, dominant negative) (Khosravi-Far *et al.*, 1995), or Ha-Ras (A15, dominant negative) (Chen *et al.*, 1994), or Green Fluorescent Protein (GFP), or p21-activated kinase (PAK) were cloned into the plasmid vector pTET7 (Hardy *et al.*, 1997). cDNAs were cloned downstream of a tetracycline repressor binding sequence, a minimal cytomegalovirus (CMV) promoter, and a transcriptional start site, and upstream of a pA sequence. The pTET7 vector also contained sites recognized by the bacterial CRE recombinase and viral packaging sequences. All plasmids generated in this study were sequenced using the dye–terminator method and checked for expression by transient transfection into HEK293 cells using the calcium phosphate method followed by Western blotting analysis, or immunofluorescence (see below). The GTPases, with the exception of dominant negative RhoA (RhoA-DN), were tagged with a myc epitope and recognized by the mAb 9E10. The RhoA-DN protein was recognized by a mAb (Santa Cruz Biochemicals, Santa Cruz, CA). The GFP protein was recognized by its fluorescence signal in the FITC channel or by polyclonal antisera (Clontech, Palo Alto, CA). PAK alleles were tagged with the hemagluttinin A epitope and recognized with the mAb 12CA5 (Boehringer Mannheim). The plasmid vector was then used to generate recombinant adenoviruses in HEK293 cells containing the CRE recombinase as described previ-

ously (Hardy *et al.*, 1997). As a result of the recombination system used, viruses generated were ~90% pure as assessed by restriction digest, and at a titer of $\sim 10^{10}$ particles/ml. Viruses were tested for function in astrocytes (see below) and subsequently plaque-purified on HEK293 cells overlaid with agar to eliminate nonrecombined or aberrantly recombined contaminants. The contaminant viruses produced no detectable effects on astrocyte morphology.

Infection of Primary Cultured Astrocytes, Organotypic Hippocampal Slices, and Live Animals

Cultures of primary astrocytes were exposed for 1 h to virus expressing a GTPase or GFP or PAK under control of tetracycline repressor elements and a minimal CMV promoter (tet-mCMV), together with virus constitutively expressing a tetracycline repressor-VP16 fusion protein, which was required to activate expression of the tet-mCMV (Gossen and Bujard, 1992; Neering *et al.*, 1996). Virus infection was performed in complete DMEM. At a multiplicity of infection (m.o.i.) of $\sim 10^7$ for both viruses, virtually all the cells in the culture expressed recombinant protein as assessed by fluorescence microscopy (see below). Cells were washed three times with complete DMEM. After the final wash, the conditioned media in which the cells had been cultured was returned together with any required growth factors. Organotypic slices were infected at identical virus titers but for a longer period (12–14 h) to allow the virus to penetrate the tissue. For live animal experiments, ~100 μl of virus diluted in complete medium was injected into the brains of halothane-anesthetized P0 rats using a syringe attached to a 27-gauge needle. Each animal was injected eight times. After injections, the animals were returned to their mother.

Immunohistochemistry

Morphological assessments were performed 12 h to 4 d after infection. Cells were fixed for 20 min at room temperature in a buffer that contained 4% formaldehyde, 320 mM sucrose, and cytoskeleton buffer (10 mM 2-(*N*-morpholino)ethanesulfonic acid, pH 6.1, 138 mM KCl, 3 mM $MgCl_2$, and 2 mM EGTA). Time-lapse microscopy during fixation confirmed that the fixation buffer had no effect on cell morphology. Cells were washed three times in cytoskeleton buffer and permeabilized for 10 min in cytoskeleton buffer supplemented with 0.5% Triton X-100. Cells were then washed in TBS (150 mM NaCl, 20 mM Tris-Cl, pH 7.4) containing 0.1% Triton X-100 (TBS-Tx) and blocked in TBS-Tx containing 2% goat serum for 1 h. For actin staining, cells were incubated with TBS-Tx containing rhodamine–phalloidin (1 μg/ml) (Molecular Probes, Eugene, OR) for 1 h, washed in TBS-Tx, washed once with water, and mounted for microscopy in antifade (Molecular Probes). For antibody staining in conjunction with actin staining, or for antibody staining alone, cells were fixed and blocked as described above, incubated with primary antibodies in TBS-Tx plus 2% goat serum for 1 h, washed five times, incubated with secondary antibodies in TBS-Tx plus 2% goat serum for 1 h, washed, and mounted as described above. The primary antibodies and concentrations used in this study were as follows: 9E10 mAb (ascites, 1:200 dilution), α-RhoA mAb (0.1 μg/ml, Santa Cruz Biochemicals), α-RhoA polyclonal antibody (0.1 μg/ml, Santa Cruz Biochemicals), α-Rac polyclonal antibody (0.1 μg/ml, Santa Cruz Biochemicals), α-Ha-Ras mAb (ascites,1:200 dilution), α-HA mAb (1 μg/ml, Boehringer Mannheim), α-GFAP mAb (ascites, 1:200 dilution; Sigma), α-GFAP polyclonal antibody (neat, Biomeda, Foster City, CA), α-GAP-43, and α-MAP-2 (ascites, 1:100 each, Sigma). Secondary antibodies and concentrations were as follows: fluorescein-conjugated α-mouse IgG1-specific antibody, which recognizes 9E10 antibody (1:500 dilution, Boehringer Mannheim), Texas Red (TR)-conjugated α-rabbit antibody (1.5 μg/ml), Cy-5–conjugated α-rabbit antibody (1.5 μg/ml), Cy-5–conjugated α-mouse antibody (1.5 μg/ml), and fluorescein-conjugated α-rabbit antibody (1.5 μg/ml) (all from Jackson Immunochemicals, West Grove, PA).

Organotypic slices were washed one time in PBS and then fixed for 45 min in cytoskeleton fixation buffer. The slices were washed for 2 h in PBS and then permeabilized and blocked overnight in PBS containing 0.5% Triton X-100 and 1% goat serum. After washing briefly in PBS–0.1% Tx, the slices were incubated overnight with 9E10 antibody ascites diluted 1:75 in α-GFAP polyclonal antibody (Biomeda Co.). The slices were washed extensively over the next 24 h with PBS–0.1%Tx, incubated overnight in fluorescein-conjugated α-mouse antibody and a Cy-5–conjugated α-rabbit antibody (each diluted 1:200 in PBS–0.1%Tx), and washed for 24 h before mounting for microscopy. Using this procedure, ~500–1000 cells were 9E10 positive, and of these roughly one-third stained definitively for GFAP and one-third were clearly GFAP negative and presumed to be neurons. Because of the relatively poor optics in the slices, no determination of cell type could be made on the remaining one-third of the cells. Attempts to visualize cells expressing the Ha-Ras-DN protein proved futile because of background problems encountered with the commercial antiserum. For whole-animal experiments, rat pups were anesthetized in a chamber containing halothane and then killed. After dissection, the brain was immersed in 10% formalin for 24 h, washed, and incubated for an additional 24 h in PBS containing 30% sucrose. The brains were then frozen under powdered dry ice and sliced in 60-μm sections on a cryostat (Leitz, Deerfield, IL). Sections of brain were stained in a manner identical to the organotypic slices.

Microscopy

Time-lapse microscopy was performed on astrocytes cultured on coverslips and grown in DMEM overlaid with mineral oil using procedures and microscopy equipment described previously (Cramer and Mitchison, 1993). Fluorescence microscopy was performed using either Zeiss Axiophot (Thornwood, NY) or Nikon (Melville, NY) microscopes. Photographs were taken on the Zeiss using conventional methods and Kodak Royal Gold 1000 film (Kodak, Rochester, NY). Images acquired on the Zeiss microscope were digitized using a Sprint-35 negative scanner (Kodak, Rochester, NY). Images were acquired on the Nikon using a charge coupled device (CCD) camera (Princeton Instruments, Monmouth Junction, NJ) driven by Win-View software package. The Nikon microscope was used for data acquisition from all samples stained with Cy-5–conjugated antibodies because infrared emissions could only be detected by the CCD camera. Images presented in Figure 9 were acquired on a Nikon Confocal Microscope driven by a Bio-Rad (Hercules, CA) software package. The images shown in Figure 9 are parfocal. All digitized images were manipulated using Adobe Photoshop 4.0. Images in Figure 7, A–D, were acquired on a Zeiss inverted microscope, which allowed the cell to be imaged in 0.4-μm z-sections. The images were acquired on a CCD camera, and light from planes not in focus was subtracted using wide-field deconvolution algorithms developed by John Sedat (University of California, San Francisco). The images were corrected for photobleaching of fluorophores that accrued during sectioning.

Data Analysis

The data presented in this article are in the form of representative images of the observed phenotypes. Each experiment was repeated a minimum of four times, and within each experiment 10–30 images were acquired and scored for the morphological phenotype in question. In general the results were uniform. Each condition tested elicited a reproducible, qualitatively similar morphology in the population of cells (e.g., after 3 d of bFGF treatment, all astrocytes in the culture grew processes of greater than two cell diameters). Quantitative measurement of such features as process length were performed in low-density cultures using IP Lab software package. The software allowed processes on digitally acquired images to be traced with a cursor and measured. Quantitation of cells from organotypic slice cultures was performed on serial sections of im-

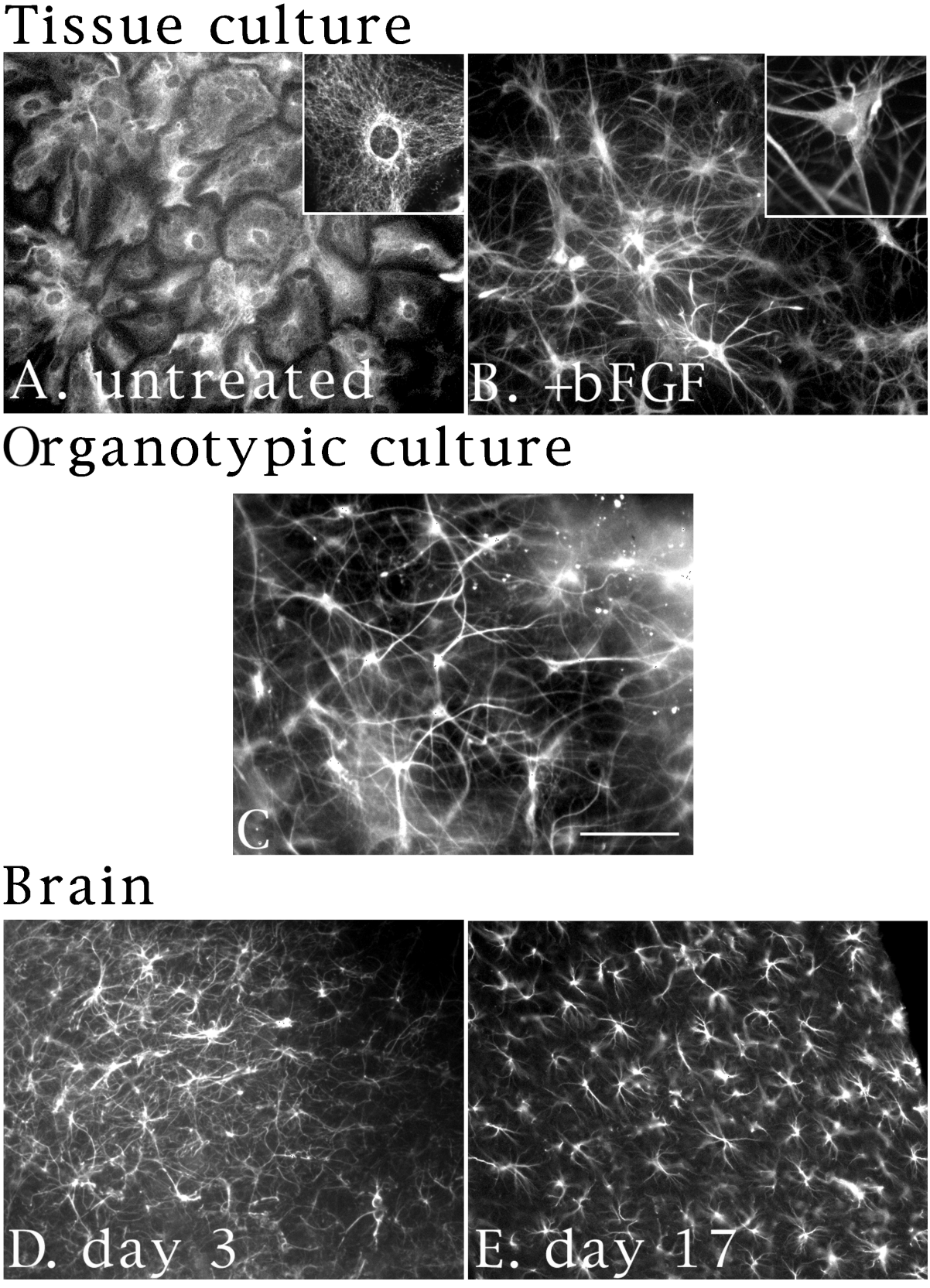
Tissue culture
A. untreated
B. +bFGF
Organotypic culture
C
Brain
D. day 3
E. day 17

Figure 1.

ages acquired on the confocal microscope. This ensured that cells scored as lacking processes did not have processes projecting orthogonally and allowed unequivocal definition of a cell as a neuron or astrocyte. Quantitation of process-bearing infected cells in slices of brain from injected animals proved more difficult. The needle penetration initiated marked angiogenesis, which autofluoresced in the FITC, rhodamine, and UV channels, although not in the infrared channel. Thus, although infected cells could be found in the Cy-5 channel, their identity as astrocyte or neuron very often could not be determined because of background autofluorescence in the other channel. As a result only a very small number of cells were counted.

RESULTS

Effects of bFGF on Morphology of CA1/CA3 Hippocampal Astrocytes

To study morphological properties of astrocytes, we established cultures from hippocampal CA1/CA3 regions derived from P0 rats. Astrocytes were the predominant cell type in the cultures (>99%) and were identified by their immunoreactivity to antibodies recognizing the intermediate filament component GFAP (Bignami *et al.*, 1972). Most GFAP-immunoreactive ($GFAP^+$) cells assumed a flattened ovoid morphology, displayed contact inhibition, and did not grow processes (>95%) (Figure 1A). Time-lapse video microscopy showed continuous elaboration of lamellipodia on the periphery of the cells (our unpublished results).

In the process of screening a panel of growth factors for effects on astrocyte morphology, we found that treatment of cultures with bFGF resulted in dramatic morphological changes in all $GFAP^+$ cells. Some of these effects with bFGF have been reported previously (Perraud *et al.*, 1988). Effects of bFGF were evident after 24 h and were complete within 48 h, affecting all $GFAP^+$ cells in the culture, as seen in Figure 1B. Using time-lapse video microscopy or α-GFAP staining, some regions of the peripheral membrane were seen to retract, whereas other regions extended to form long processes that grew across apposing cell bodies and other processes. Time-lapse microscopy ruled out the possibility of a subpopulation of process-bearing cells overtaking the culture. Quantitation of process lengths confirmed that bFGF caused process growth beyond the original boundaries of the cell. By contrast, dibutyryl cyclic AMP (dbcAMP) caused process formation as a result of membrane retraction but not growth, in general agreement with previously published reports (Goldman and Abramson, 1990; Baorto *et al.*, 1992). After 2.5 d of bFGF treatment, process lengths ranged from 9 to 223 μm and averaged 62.4 $\pm$ 1.3 μm (SEM; n = 634). By contrast, processes elicited with 2 mM dbcAMP ranged from 8 to 116 μm and averaged 42 $\pm$ 0.8 μm (SEM; n = 516) in length, equivalent to the radius of untreated cells (mean, 40 $\pm$ 0.8 μm [SEM], n = 83; range 22–55 μm). The difference in mean process length between cells treated with bFGF and dbcAMP and the difference between process length of bFGF-treated cells and the radii of untreated cells were statistically significant ($p < 0.001$; two-tailed t test). In contrast, the difference between process length of dbcAMP-treated cells and radii of untreated cells was not significant ($p < 0.3$).

The bFGF-induced processes of $GFAP^+$ cells remained refractory to staining with neuronal markers such as GAP-43 or MAP-2. Actin staining revealed both filopodia and lamellipodia at the tips of processes and along their lengths (Figure 2, E and F), a feature not evident with dbcAMP treatment. The $GFAP^+$ cells continued to exhibit these morphological changes even after long-term exposure to bFGF (up to 10 d, the longest time measured), and effects persisted for several days after removal of bFGF. Another noteworthy feature of the bFGF phenotype was the remarkable resemblance between the morphology of the processes in cultured cells treated with bFGF and the morphology of $GFAP^+$ cells in organotypic slice cultures (Figure 1C), and in brains from P3 (Figure 1D) or P17 animals (Figure 1E). Treatment of cells with other growth factors, such as PDGF, NGF, TGF-β, or leukemia inhibitory factor, produced no detectable morphological changes. EGF, however, produced morphological changes indistinguishable from those observed with bFGF, although with a somewhat slower time course.

Cytoskeletal Rearrangements Underlie bFGF-induced Morphological Changes

To determine whether cytoskeletal proteins participate in the morphological changes observed with bFGF treatment, we visualized actin, tubulin, and the intermediate filament protein GFAP in bFGF-treated and untreated astrocytes. Figure 2, A–F, illustrates the effects of bFGF on the actin cytoskeleton at low (A, C, E) and high magnification (B, D, F). In untreated cells, actin was organized in bundles that extended in long parallel bands across the cells (Figure 2, A and B). In cells treated with bFGF for 1 d, the actin bundles were much less apparent (Figure 2, C and D) and had lost much of their parallel orientation. This actin reorganization occurred in areas where the membrane was retracting (Figure 2D, r). In addition such reorganiza-

Figure 1 (facing page). bFGF induces processes in hippocampal CA1/CA3 astrocytes. (A and B) Images of astrocytes cultured for 1 wk and left untreated (A) or treated with bFGF (20 nM) for 2 d (B). Cells were stained with a polyclonal α-GFAP antibody and a FITC-conjugated secondary antibody. Insets are higher-magnification images of identically stained cells. (C) Images of hippocampal astrocytes grown in organotypic slice cultures. After 3 d, cells were fixed and stained with a polyclonal α-GFAP antibody and a Cy-5–conjugated secondary antibody. (D and E) Images of astrocytes from brains of P3 (D) or P17 (E) animals. Brains were fixed and sectioned, and then stained as in C above. Bar (in C): A, B, D, and E, 20 μm; C and insets in A and B, 10 μm.

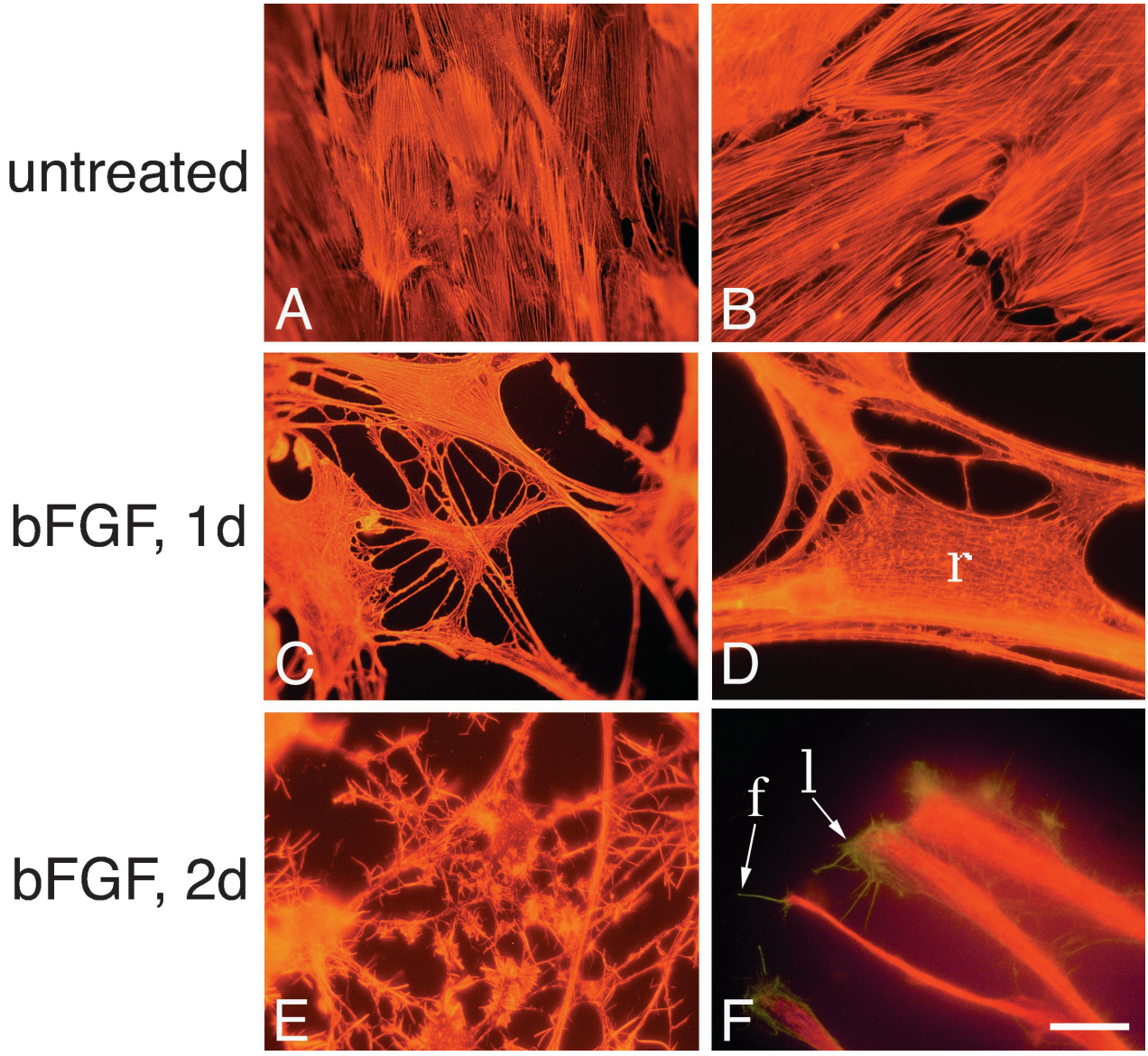

Figure 2. bFGF induces actin bundles to disassemble in retracting areas but not in processes. (A–F) Images of astrocytes left untreated (A and B) or treated with bFGF for 1 d (C and D) or 2 d (E and F) and stained with rhodamine–phalloidin (A–E) or with rhodamine–phalloidin, α-GFAP, and a Texas Red (TR)-conjugated secondary antibody (F). f and l in F refer to filopodia and lamellipodia, respectively. r in D denotes retracting area. Bar (in F): A, C, and E, 32 μm; B, D, 12.5 μm; F, 10.5 μm.

tion was evident in cells that had not yet developed processes nor progressed beyond the initial stages of retraction. In cells treated for 2–3 d with bFGF (Figure 2, E and F), actin stained robustly in long fibers that extended the length of the processes. Actin staining also revealed the presence of filopodia and lamellipodia (Figure 2F, f and l, respectively) at the tips of and along the processes (see also Figure 2E). These structures did not contain GFAP filaments (Figure 2F). Thus, with bFGF treatment, actin bundles appeared to be localized to extending processes but not to retracting areas.

To determine whether actin disassembly alone could account for the morphological changes observed with bFGF, we treated cells with cytochalasin D (Baorto *et al.*, 1992), which causes net actin depolymerization by blocking polymerization. Within 30 min, cytochalasin D treatment resulted both in loss of actin bundles and in membrane retraction. Although cytochalasin D treatment did produce short processes

from retracted membrane, these processes did not extend, and filipodia and lamellipodia were not evident. Process growth could not be assessed over longer time courses (>3 h), however, because of the toxicity of cytochalasin D. Thus, net actin depolymerization appears sufficient to produce the bFGF-induced morphological changes associated with membrane retraction but does not appear to account for process growth.

Other cytoskeletal elements, such as GFAP or tubulin, might participate with actin in the process growth induced by bFGF. Both GFAP and tubulin filament width increased before membrane retraction, becoming less apparent in retracting areas, and later extended into developing processes (for GFAP, compare insets in Figure 1, A and B); however, changes in actin appeared to precede changes in other filaments.

Effects of Ras Family GTPases on Astrocyte Morphology

Effects of Rac1 GTPase

To determine whether bFGF acted through Ras family GTPases to cause the observed morphological changes, we set out to express various alleles of *rac1*, *rhoA*, or *Ha-ras* GTPases. These included alleles encoding wild-type proteins, proteins with severely diminished GTP hydrolysis rates (activated, *), and proteins with diminished capacity either to bind guanine nucleotides or to exchange GDP for GTP (DN). All the GTPases reported in this article except the RhoA-DN were tagged at the amino terminus with a myc epitope, allowing detection of the protein by immunofluorescence with the 9E10 mAb (Ramsay *et al.*, 1984). In cases where myc-tagged and untagged versions of the same allele were compared, no phenotypic differences were observed. RhoA-DN, as well as the myc-tagged alleles, could be detected with commercially available antisera (see MATERIALS AND METHODS). Detection of endogenous proteins with the commercial antisera revealed staining near background levels.

Because primary astrocytes are refractory to conventional transfection or retroviral infection protocols, we constructed recombinant adenoviruses expressing the GTPase alleles under control of the tetracycline promoter system (Gossen and Bujard, 1992; Hardy *et al.*, 1997). This system required coinfection with a second recombinant adenovirus constitutively expressing the tetracycline repressor-VP16 fusion protein (tetracycline transactivator) to activate GTPase transcription (Neering *et al.*, 1996). Expression of the GTPases could be repressed by addition of tetracycline. Adenovirus infection of astrocytes proved extremely efficient. Greater than 95% of the cells could be induced to express recombinant proteins by using virus at a high m.o.i. At lower m.o.i., only a fraction became infected. Adenovirus infection per se, or expression of control proteins such as GFP (Figure 4, J–L), the PAK, or tetracycline transactivator alone, was not toxic within 4 d after infection and did not disrupt the bFGF effect (Figure 4, J–L) or cause cytoskeletal changes.

Infection of astrocytes with adenovirus expressing Rac1-DN caused dramatic morphological changes resembling those observed with bFGF. Figure 3 shows a time course of the effects of Rac1-DN on cell morphology and the actin cytoskeleton. One day after infection, membrane retraction and process growth beyond the original cell boundaries were evident in some but not all infected cells (Figure 3A). Cytoskeletal changes similar to those observed with bFGF treatment were also apparent at this time point even in infected cells without processes. Specifically, the GFAP filaments appeared thicker in some areas of the cell and less apparent in others (Figure 3B). Moreover, actin bundles dispersed in the cell body as exemplified in Figure 3, C and D. The Rac1-DN–expressing cell at the left, identified by 9E10 staining in Figure 3C, has only a skeletal actin network, compared with the uninfected cell on the right (Figure 3D; higher magnification).

Two to three days after infection, most Rac1-DN–infected cells (~80%) had contracted, had extended processes well beyond their initial boundaries, and had achieved a morphology generally similar to that of bFGF-treated cells (Figure 3, E and F). Processes elicited with Rac1-DN ranged from 10 to 197 μm and averaged 57 $\pm$ 2 μm (SEM; n = 248) in length. The difference between process length of Rac1-DN cells and the radii of untreated cells was statistically significant ($p < .001$; two-tailed t test). Processes stained strongly for GFAP and actin (Figure 3, F and H, respectively), and filopodia were evident (Figure 3, G and H). Some differences between bFGF and Rac1-DN were apparent. In Rac1-DN–infected cells, lamellipodia were generally absent, consistent with effects reported with this allele in other cell types (Ridley *et al.*, 1992). Also, highly branched processes were initially conspicuous but became less apparent after several days.

To determine whether inhibition of Rac1 or a Rac1-like protein was necessary for bFGF's effects, we next expressed Rac1*. The effects of Rac1* on untreated or bFGF-treated astrocytes are shown in Figure 4. Cells infected with adenovirus (Ad)-Rac1* were recognized by 9E10 staining (Figure 4A) and identified as astrocytes by GFAP staining (Figure 4B). Infected cells showed no detectable morphological alterations when compared with uninfected cells in the same culture (Figure 4C). When treated with bFGF (Figure 4, D–F), infected cells (Figure 4D) showed no evidence of process growth compared with uninfected cells in the same culture (Figure 4, E and F), and actin staining revealed actin bundles reminiscent of uninfected cells.

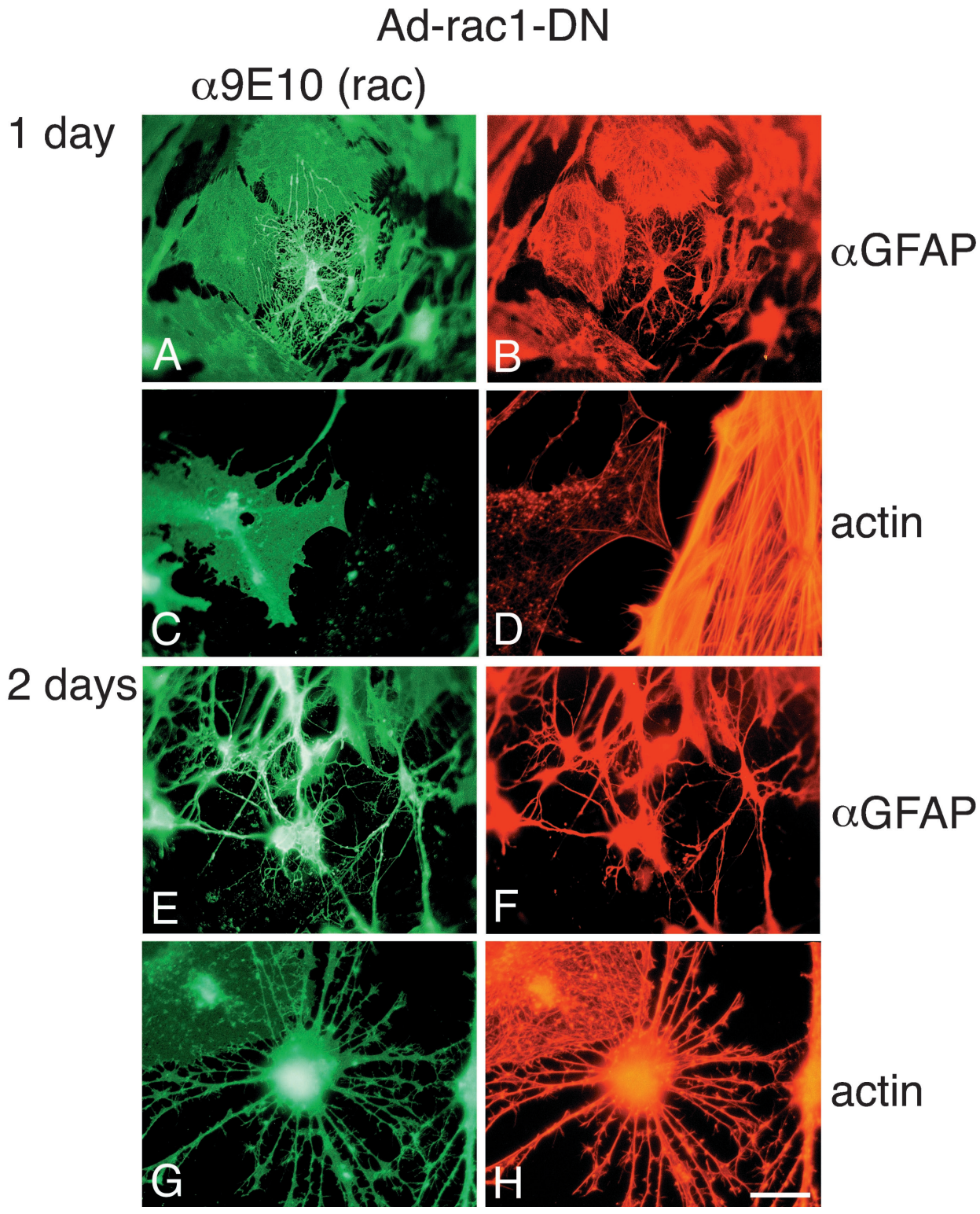

Figure 3. Rac1-DN causes morphological differentiation and actin bundle reorganization. Images of astrocytes infected with Ad-Rac1-DN and Ad-tetR-VP16 at high m.o.i. for 1 d (A–D) or 2 d (E–H), and stained with 9E10 and a secondary fluorescein-conjugated antibody to detect Rac1-DN (A, C and E), together with either α-GFAP and a TR-conjugated secondary antibody to identify the cells as astrocytes (B and F), or rhodamine–phalloidin (D and H). Bar (in H): A–C, E, and F, 27 μm; D, G, and H, 11 μm. Note that C and D are low- and high-magnification images, respectively, of the same cells. The cell on the left in C and D expresses Rac1-DN.

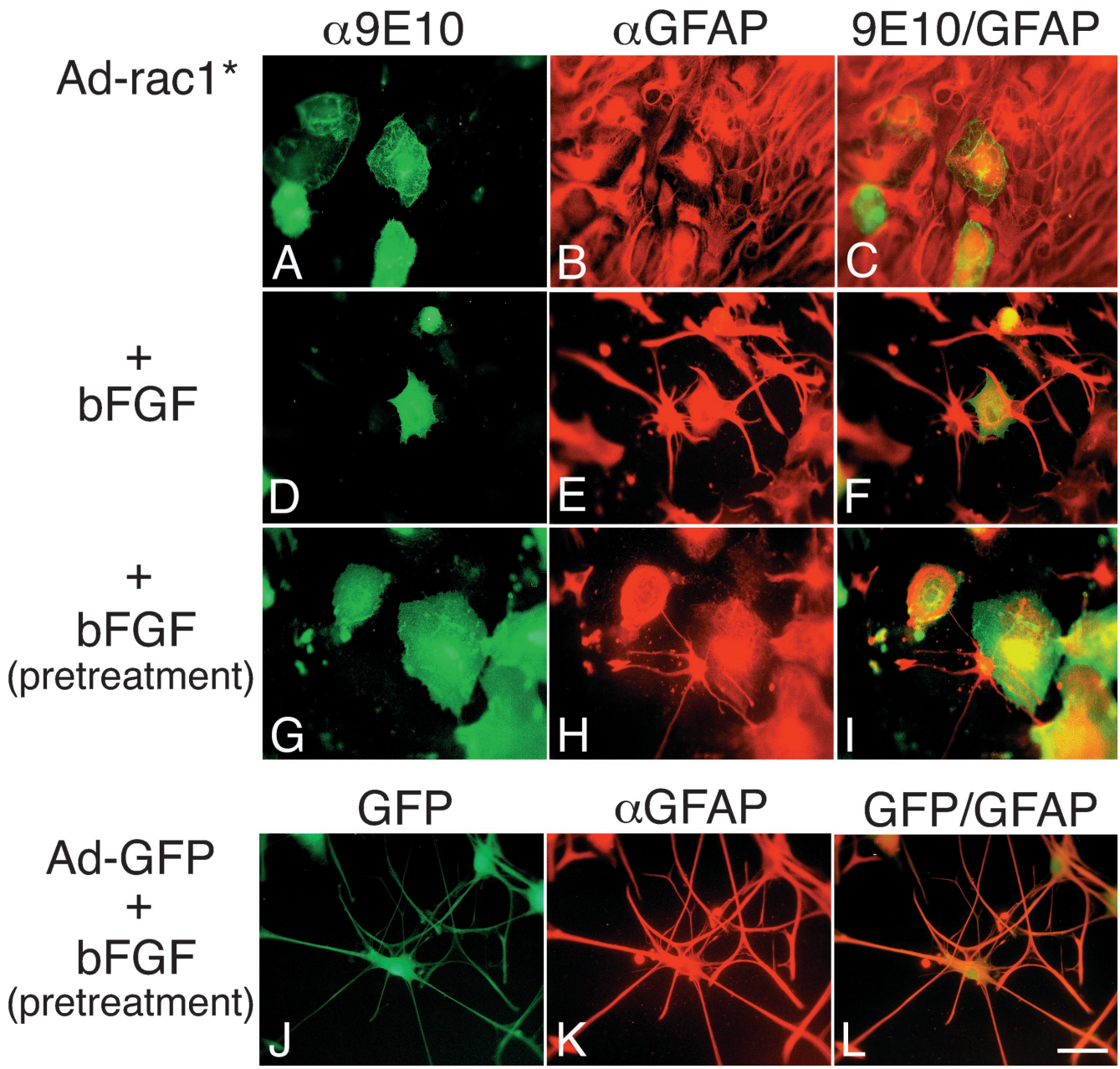

Figure 4. Rac1* blocks and reverses bFGF-induced morphological changes. (A–F) Images of cells infected with Ad-Rac1* and left untreated (A–C) or treated with bFGF (D–F) for 2 d. Cells were stained with 9E10 and a fluorescein-conjugated secondary antibody to identify recombinant protein (A and D), together with α-GFAP and a TR-conjugated secondary antibody to identify the cells as astrocytes (B and E). Double exposures are shown in C and F. Note that uninfected cells in E have processes. The cells in A–C are from 3-wk-old cultures that exhibited some spontaneous morphological changes. (G–L) Images of cells that were pretreated with bFGF for 1 wk and then infected for 2 d with Ad-Rac1* (G–I) or Ad-GFP (J–L) and maintained in bFGF. G–I were stained as in A–F. J–L were stained only with the α-GFAP/TR secondary antibody. GFP is visible in the fluorescein channel (J). Double exposures are shown in I and L. Bar, 25 μm.

There was a subtle difference between the radii of untreated cells (mean, 40 ± 0.8 μm) and those of Rac1*-infected cells treated with bFGF (mean, 33 ± 1 μm [SEM], n = 39; range 20–53 μm). This difference may be attributable to partial block by Rac1* in some cells in conjunction with a differential sensitivity of membrane retraction and process growth to the effects of Rac1*. In general, however, we could find no Rac1*-infected cells that exhibited processes with bFGF treatment, whereas nearly all uninfected cells did.

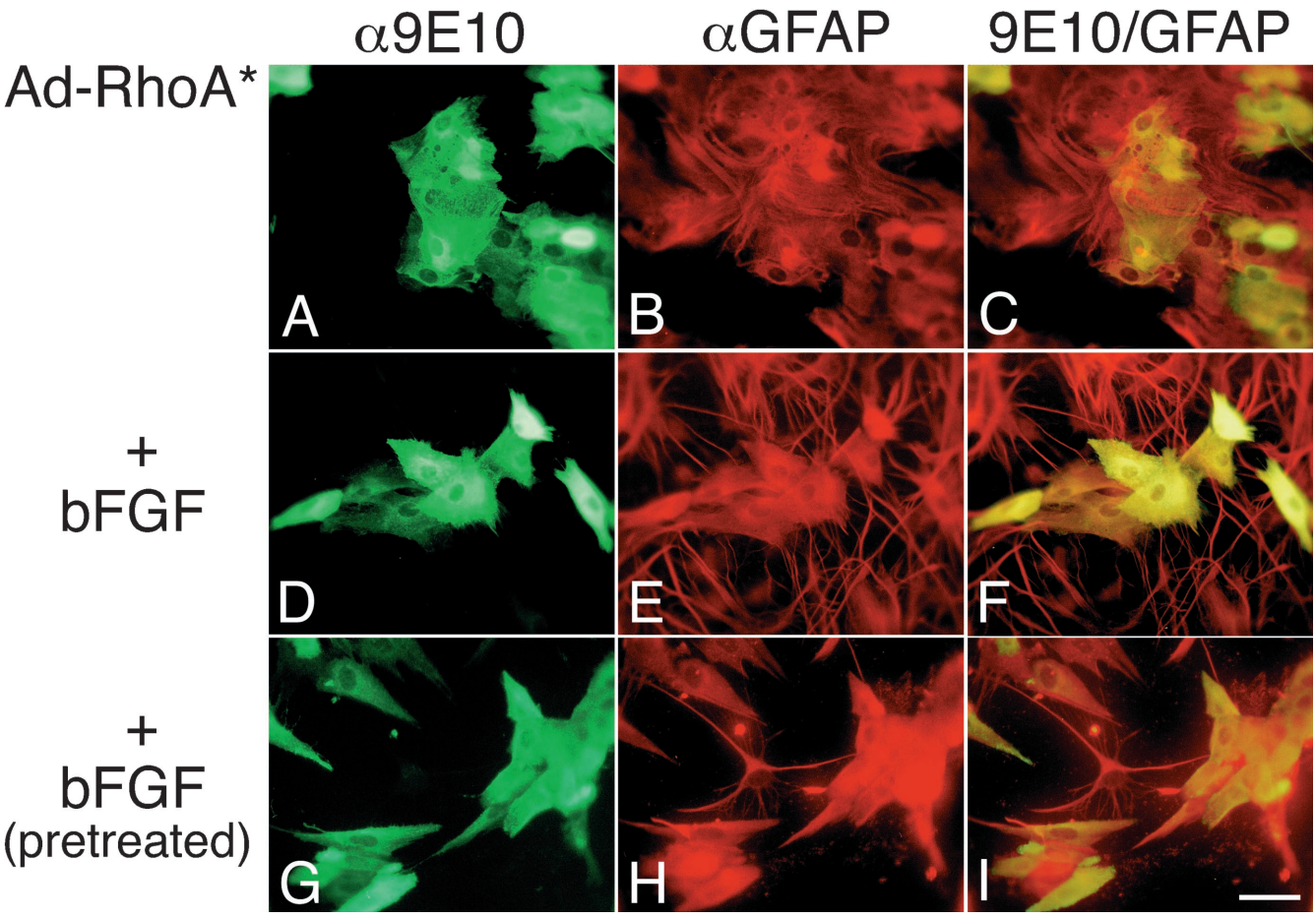

Figure 5. RhoA* blocks and reverses bFGF-induced morphological changes. (A–F) Images of cells infected with Ad-RhoA* and left untreated (A–C) or treated with bFGF for 3 d (D–F). Infected cells were recognized by 9E10/FL staining (A and D), and the cells were identified as astrocytes by GFAP/TR staining (B and E). C and F are double exposures. (G–I) Images of cells pretreated with bFGF for 1 wk and then infected for 2 d with Ad-RhoA* and maintained in bFGF. G–I were stained as in A–F. I is a double exposure. Bar, 25 μm.

Rac1* also reversed bFGF effects. When cells pretreated with bFGF for 1 wk were infected with Ad-Rac1*, the cells retracted or lost their processes, flattened out, and assumed a morphology reminiscent of untreated, uninfected cells (Figure 4, G–I). Uninfected cells in the same culture retained their differentiated characteristics (Figure 4I). Infection of bFGF-pretreated cells with Ad-GFP produced no change (Figure 4, J–L). Together, these results suggest that inhibition of endogenous Rac1 or a Rac1-like activity is necessary and sufficient to initiate and maintain bFGF-dependent morphological changes in culture.

Effects of RhoA GTPase

Because the morphological changes induced by bFGF required the reorganization of actin bundles, we next asked whether the effects of bFGF could be antagonized by agents that cause actin bundle formation. We decided to test the effects of RhoA because it catalyzes actin stress fiber and bundle formation in several cell types and because it acts downstream of both growth factors and Rac1 as part of a GTPase cascade in Swiss 3T3 fibroblasts (Ridley and Hall, 1992).

Expression of RhoA* in untreated astrocytes had little effect on cell morphology (compare infected cells [9E10 staining, Figure 5A] with $GFAP^+$ cells [Figure 5, B and C]); however, RhoA* had dramatic effects on bFGF-induced morphological changes (Figure 5, D–I). With bFGF treatment, RhoA*-infected cells remained flat and without processes (9E10 staining, Figure 5D) compared with uninfected cells in the culture (Figure 5, E and F). Moreover, there was little difference between the radii of untreated cells and those of RhoA*-infected cells treated with bFGF (mean, 39 ± 1 μm [SEM], n = 60; range 23–63 μm). Among the bFGF-treated cells, RhoA* infection led to dramatic actin bundle formation similar to that observed in untreated cells (Figure 2, A and B). Moreover, GFAP staining

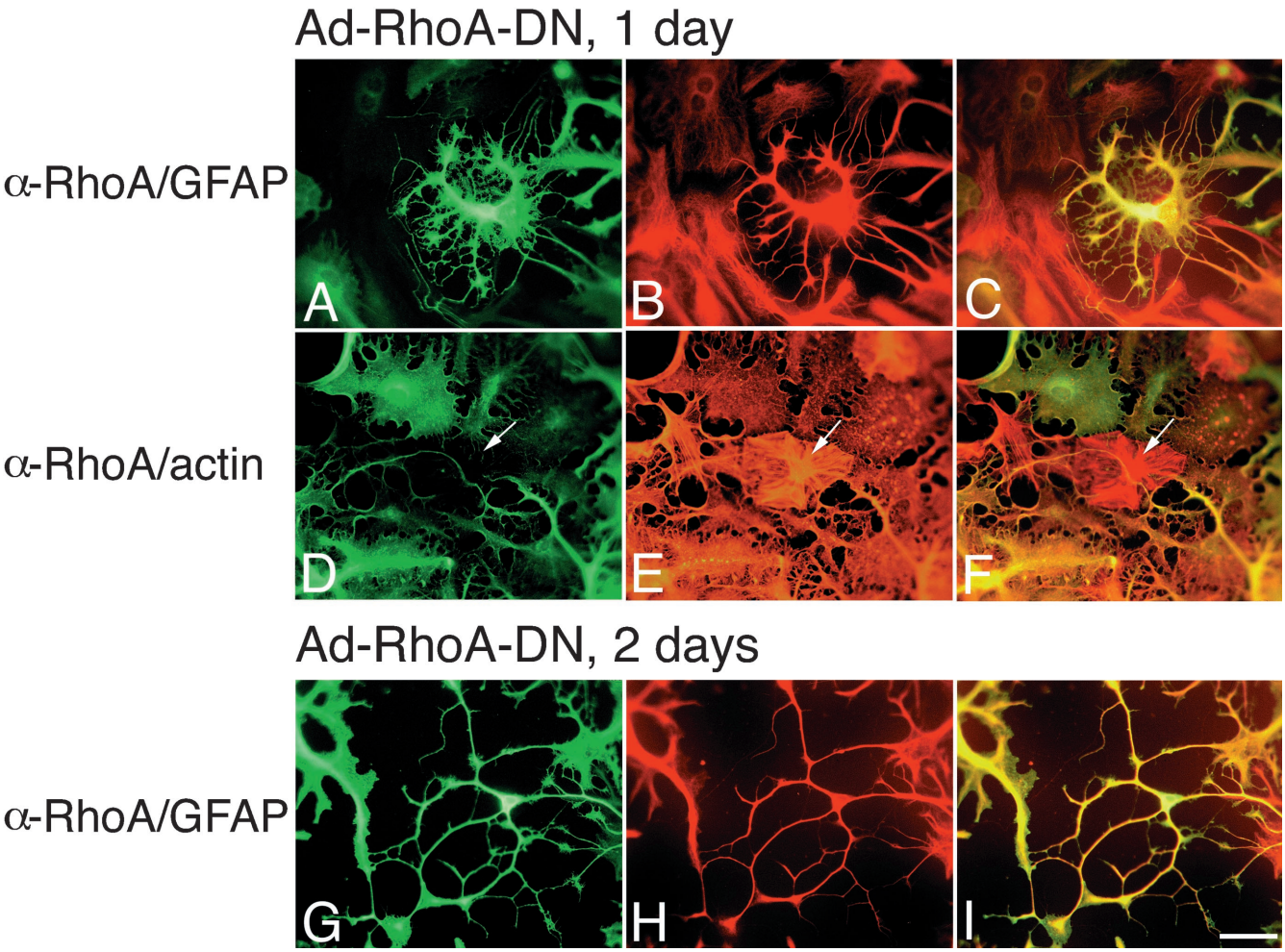

Figure 6. RhoA-DN induces morphological differentiation of astrocytes. (A–F) Images of cells infected with Ad-RhoA-DN at high m.o.i. for 1 d. (A–C) Images of cells stained with α-RhoA antibody/FL conjugate to recognize infected cells (A) together with α-GFAP/TR conjugate to identify the cells as astrocytes (B). (D–F) Images of cells stained with α-RhoA antibody/FL conjugate (D) together with rhodamine–phalloidin to recognize actin (E). C and F are double exposures. Note that the uninfected cell in the center of the image in D–F (arrow) has actin fibers (E). (G–I) Images of cells infected for 2 d with Ad-RhoA-DN and stained with α-RhoA/FL (G) together with α-GFAP/TR (H). Bar, 25 μm.

was diffuse in infected cells rather than bundled (compare noninfected and infected cells in Figure 5, E and F). RhoA* also caused bFGF-pretreated process-bearing cells to revert to flattened cells without processes (Figure 5G), whereas uninfected cells (Figure 5, H and I) or Ad-GFP infected cells (Figure 4, G–I) remained process bearing.

These results suggest that actin bundle reorganization was necessary for the morphological changes produced by bFGF, and that a RhoA-like protein might be responsible for maintaining actin bundles in untreated cells. To determine whether inhibition of RhoA or a RhoA-like protein was necessary for bFGF's effects, we next expressed RhoA-DN in astrocytes. RhoA-DN produced effects generally similar to those of bFGF or Rac1-DN, although the processes were somewhat longer (mean, 76 ± 3.5 μm [SEM], n = 142; range 20–228 μm). A time course of RhoA-DN effects on morphology is shown in Figure 6. One day after infection, RhoA-DN caused membrane contraction and GFAP bundling (Figure 6, A–C) and a general loss of somatic actin bundle staining (Figure 6, D–F). After 2 d, pronounced membrane retraction was evident, and cells extended long processes containing bundled GFAP filaments (Figure 6, G–I) and actin. bFGF treatment of RhoA-DN–infected cells produced no additional changes. Although processes produced by RhoA-DN were ultimately indistinguishable from those seen with bFGF or Rac1-DN, some early differences were apparent. In particular, RhoA-DN initially produced fivefold thicker processes than those observed with bFGF or Rac1-DN.

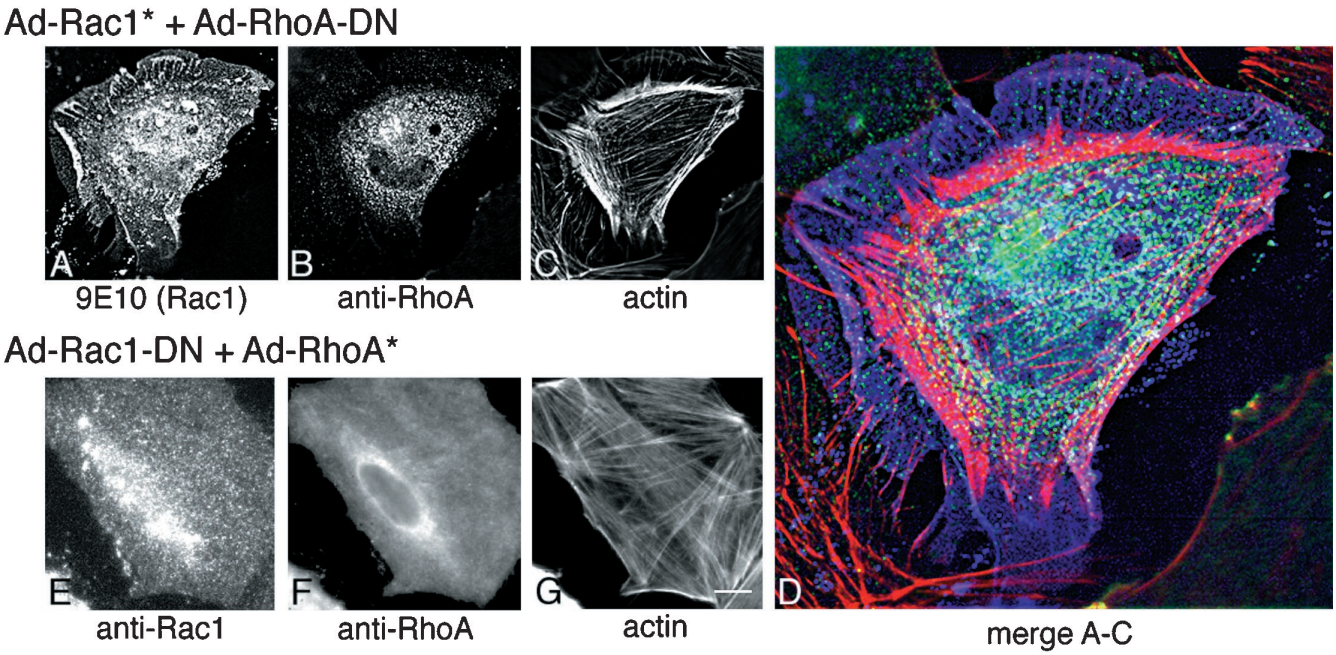

Figure 7. Effects of GTPase combinations on astrocyte morphology. (A–D) Images of cells infected with Rac1* plus RhoA-DN. Images are composed of light from a 0.4-μm-thick parfocal z-section. Out of focus light from above and below this section were eliminated using wide-field deconvolution algorithms (see MATERIALS AND METHODS). Infected cells were recognized by staining with 9E10/fluorescein conjugate to recognize Rac1* (A) together with α-RhoA/Cy-5 conjugate (B) and rhodamine–phalloidin (C). These three images are merged in D. Rac1 is pseudocolored blue, RhoA is pseudocolored green, and actin is pseudocolored pink. The RhoA-DN was not epitope-tagged, so the 9E10 antibody could be used to detect Rac1*. Note that the actin is concentrated in the cell periphery, RhoA-DN is restricted to the cell interior, and Rac1* is uniformly distributed throughout the cell. (E–G) Images of cells infected with Rac1-DN plus RhoA*. Cells were stained with α-Rac/FL conjugate to recognize the Rac1-DN protein together with α-RhoA/Cy5 conjugate to recognize the RhoA* protein. The presence of a myc epitope tag on both protein types obviated the use of the 9E10 antibody. Note that the actin bundle staining in G resembles untreated cells. E–G were photographed using a standard microscope. Bar (in G): A–C, G–I, 8 μm; D, 3.3 μm.

Effects of combinations of Rac1 and RhoA GTPases

The observation that Rac1* and RhoA* blocked and reversed bFGF-induced changes led us to next ask whether Rac1* could reverse RhoA-DN effects and whether RhoA* could reverse Rac1-DN effects. Images of cells infected with combinations of RhoA and Rac1 viruses are shown in Figure 7. Cells infected with either Rac1* plus RhoA-DN (Figure 7, A–D), or Rac1-DN plus RhoA* (Figure 7, E–G) failed to grow processes or undergo membrane retraction. There were, however, some notable differences in actin bundling patterns (compare Figure 7, C and D, with G). Cells infected with Rac1-DN plus RhoA* showed actin bundles identical to those observed in cells infected with RhoA* alone (Figure 7G). In contrast, actin bundles in cells infected with RhoA-DN plus Rac1* localized to the periphery of the cell (Figure 7C). Although actin appeared concentrated, GFAP staining remained diffuse. These results suggest that actin reorganizes to the cell periphery during process formation. Inhibition of RhoA appears to redistribute actin to the periphery, and the level of Rac1 activity appears to regulate whether actin can polymerize at sites of process formation or organize into processes.

The altered actin distribution seen with this combination of viruses may have resulted from the localization of RhoA-DN to the cell center and only to a small extent in the periphery (Figure 7B). The activated RhoA allele showed no such localization (Figure 7F) nor did either activated or dominant negative alleles of Rac1 (Figures 7, A and E). Coplanar images generated using wide-field deconvolution microscopy (see MATERIALS AND METHODS) and shown in Figure 7, A–D, confirmed that the apparent localization of RhoA-DN (Figure 7, B and D) reflected an increased concentration of protein in the cell center and not a relative increase in fluorescence caused by a larger volume in the cell center compared with the periphery. We could only observe such localization of RhoA-DN in the context of Rac1* expression because RhoA-DN was not excluded from growing processes (Figure 5).

Effects of Ha-Ras GTPase

Recent reports have suggested that the Ha-Ras GTPase can activate Rac1 and mediate growth factor effects on Rac1 in various cell types (Ridley *et al.*, 1992). To determine whether Ha-Ras mediated bFGF's

morphological effects, we constructed an adenovirus that expresses Ha-Ras^{15ala} (Ha-Ras-DN), a mutant Ha-Ras protein with severely compromised capacity to load any guanine nucleotide which functions as a dominant negative (Chen *et al.*, 1994). As shown in Figure 8, expression of Ha-Ras-DN had no detectable effects on astrocyte morphology by itself (Figure 8, A and B); however, Ha-Ras-DN expression was sufficient to block bFGF-induced morphological changes (Figure 8, C and D). Ha-Ras-DN appeared to block only bFGF-induced effects. Expression of equivalent levels of Ha-Ras-DN failed to block Rac1-DN–induced effects (Figure 8, E and F) or RhoA-DN–induced effects (Figure 8, G and H). Together, these results suggest that Ha-Ras mediates bFGF effects and functions upstream of Rac1 and RhoA.

Effects of RhoA and Rac1 GTPases in Organotypic Cultures

We next set out to test the possibility that a GTPase cascade similar to the one used by bFGF to produce processes in dissociated cultures of astrocytes might also be used in the more physiological setting of organotypic cultured brain tissue. Our data with the activated RhoA and Rac1 (Figures 4 and 5) show that these GTPases not only inhibit but also reverse the bFGF effect. Thus, low levels of Rac1 and RhoA appear to be required not only to initiate but also to maintain processes. A role for these GTPases in process maintenance allowed us to assess the effects of activated alleles of Rac1 and RhoA on astrocytes in organotypic hippocampal slice cultures. As in the tissue culture experiments above, infected cells were detected by 9E10 staining, and their identity as astrocytes was confirmed by GFAP staining. As shown in Figure 9, both Rac1* and RhoA* caused astrocytes to lose their processes (a in Figure 9, C and E). Rac1* and RhoA* also had detectable although different effects on neurons in the slices (n in Figure 9, D and insets in E). Rac1* had no gross effect on neuronal processes (n in Figure 9D) but did appear to cause an increase in filopodial-like structures on neuronal processes in some cells. RhoA*, by contrast, caused neurons to retract their processes (Figure 9E, insets). Staining with neuronal markers such as MAP2 confirmed that process-bearing cells that remained unaffected by Rac1* were indeed neurons. Likewise, some RhoA*-expressing cells lacking processes stained with MAP2. These effects on neurons are not inconsistent with previous reports for both Rac1 and RhoA in cultured neuronal cell types (Kozma *et al.*, 1997; Leeuwen *et al.*, 1997; see however, Threadgill *et al.*, 1997) or in brain (Luo *et al.*, 1996). By contrast, GFP had no detectable effect on either astrocytes (a in Figure 9A) or neurons (n in Figure 9B). On counting cells expressing GFAP, we found that only 11.7% (n = 60 cells) of those additionally expressing Rac1*, and 8.3% (n = 60 cells) of those additionally expressing RhoA*, exhibited processes longer than one cell diameter. By contrast all cells expressing GFP and GFAP had processes exceeding one cell diameter in length (n = 60 cells). For neurons, identified by MAP2 staining, nearly all Rac1*-expressing cells (98%; n = 60 cells) or GFP-expressing cells (100%; n = 30 cells) displayed processes compared with only 10% (n = 30 cells) for RhoA*-expressing cells. Qualitatively similar results were obtained in live animals infected with these viruses (our unpublished results).

DISCUSSION

bFGF Causes Process Growth and Membrane Retraction in Dissociated Primary Culture

We have shown that treatment of primary cultured astrocytes with bFGF results in membrane retraction accompanied by the extension of actin-rich processes that bear a strong morphological resemblance to GFAP$^+$ astrocytes in animals (Figure 1, D and E) (see also Misson *et al.*, 1991) and in hippocampal organotypic slice cultures (Figure 1C). Our results suggest that bFGF acts through a signal transduction cascade involving the Ha-Ras, Rac1, and RhoA GTPases to cause membrane retraction and process growth. These gross morphological changes appear to result from actin reorganization in the cell soma and actin polymerization in the growing processes. The changes in the actin cytoskeleton precede reorganization of other cytoskeletal elements such as GFAP and tubulin.

What is the relationship between membrane retraction and process growth? Baorto *et al.* (1992) reported that dbcAMP, a membrane-permeable cAMP analogue, induced actin bundle disassembly and membrane retraction (or "cavitation"), and as a consequence, "process" formation. Our results show that bFGF, Rac-DN, and RhoA-DN cause not only membrane retraction but also process growth and extension. Thus, process lengths were up to 1.8-fold longer with bFGF or the DN GTPases compared with dbcAMP and the radii of untreated cells. Although processes clearly form coincidentally with membrane retraction in our study (Figures 2 and 3G), we often observed process growth in cells whose membranes had not yet retracted (Figure 3C). Therefore, process growth and membrane retraction appear to occur independently, although our results suggest that somatic actin bundles themselves must reorganize for growth to occur. Our finding that actin filaments assemble in growing processes further suggests that reorganization of actin bundles is not uniformly controlled throughout the cell.

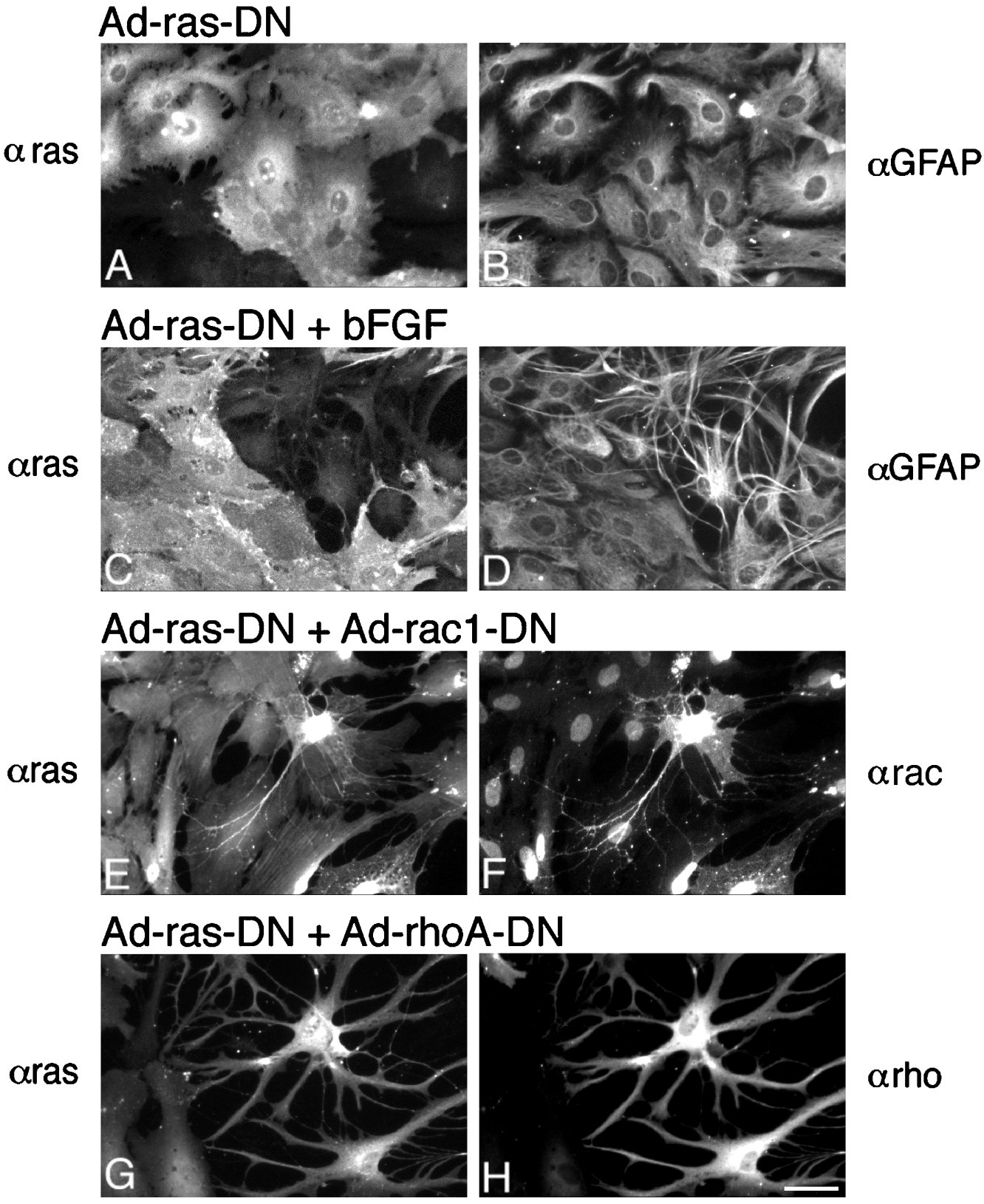
Ad-ras-DN
αras
αGFAP
A
B
Ad-ras-DN + bFGF
αras
αGFAP
C
D
Ad-ras-DN + Ad-rac1-DN
αras
αrac
E
F
Ad-ras-DN + Ad-rhoA-DN
αras
αrho
G
H

Figure 8.

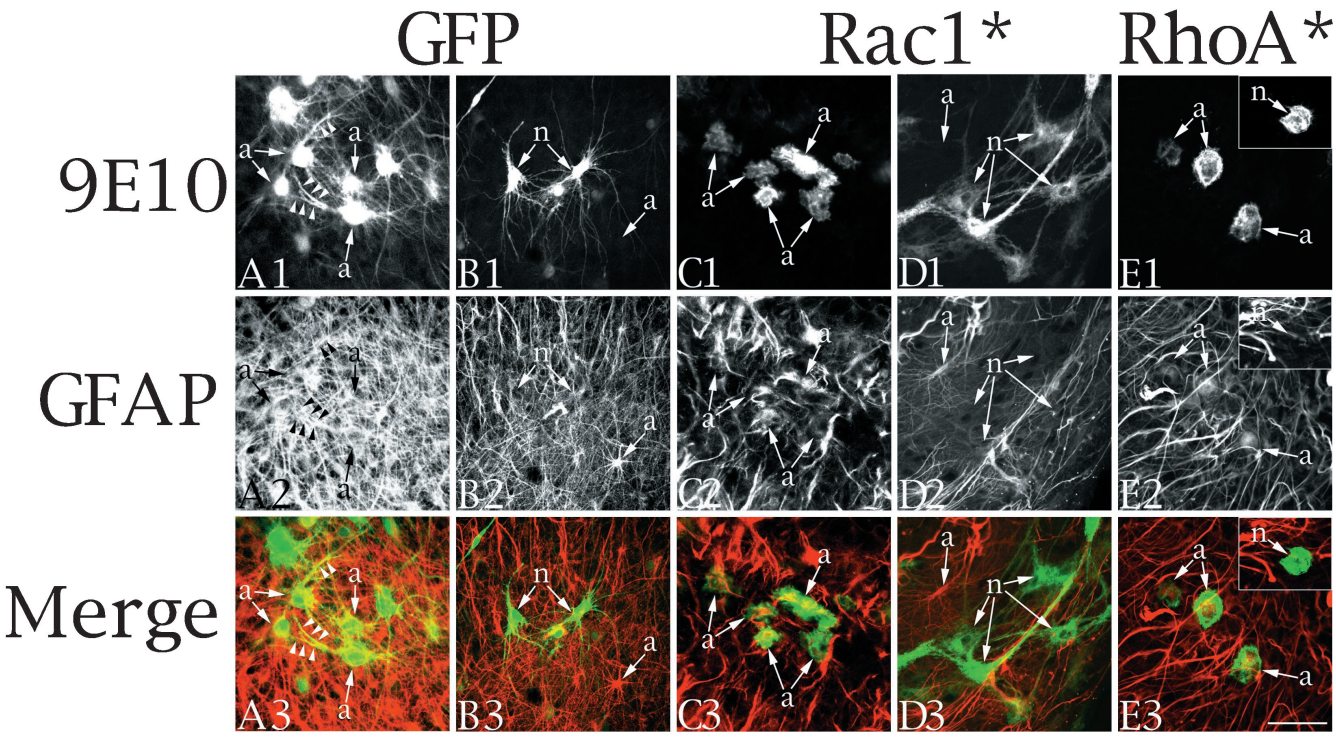

Figure 9. Effects of Rac1* and RhoA* on process growth in neurons and astrocytes in cultured organotypic hippocampal slices. (A1–A3 and B1–B3) Confocal images of cells from organotypic slices infected for 2 d with Ad-GFP and stained with 9E10/FITC (A1 and B1) together with GFAP/Cy5 (A2 and B2) to identify the cells as astrocytes. Cells labeled "a" (astrocytes) are identifiable in the GFAP/Cy5 channel, whereas cells labeled "n" (neurons) were not. Other experiments confirmed that GFAP-negative cells stained with neuronal markers such as MAP2. Images in A1 and B1 result from GFP fluorescence and not 9E10 staining because uninfected cultures had no signal in any plane in the FITC channel. Images from the top row (A1–E1) were pseudocolored green, and images from the middle row (A2–E2) were pseudocolored red. The pseudocolored images were combined to generate the merged image in the third row (A3–E3). (C1–C3 and D1–D3) Confocal images of cells from organotypic cultures infected for 2 d with Ad-Rac1* and stained as above. Rac1* causes loss of processes on astrocytes (a in C) but not on neurons (n in D). The neurons are not evident in the GFAP/Cy5 channel (D2). (E1–E3) Confocal images of cells from organotypic cultures infected with Ad-RhoA* and stained as above. Note that RhoA* causes loss of processes on astrocytes (a). Insets illustrate the effects of RhoA* on neurons. n in the inset identifies a cell lacking processes that is not evident in the GFAP channel (E2 inset).

bFGF Initiates a GTPase Cascade

How do Ha-Ras, Rac1, and RhoA GTPases cause actin reorganization and the consequent process growth and membrane retraction? Figure 10 shows a general model consistent with all of our data. A central feature of this model is that in untreated cells, Rac1 and RhoA have high basal activity, perhaps as a result of serum in the media, which leads to lamellipodia at the periphery and actin bundles across the soma. Our data with dominant negative and activated alleles of Rac1 and RhoA (Figures 3–6) provide evidence that these GTPases inhibit membrane retraction and process growth, either directly or via the actin structures they produce. bFGF causes process growth and membrane retraction by relieving this inhibition. Experiments with the combinations of Ha-Ras, Rac1, and RhoA alleles (Figures 7 and 8) define Ha-Ras as an upstream inhibitor of Rac1 and Rac1 as an upstream activator of RhoA (see below). Thus, bFGF acting through the Ha-Ras GTPase causes inhibition of the Rac1 GTPase, which in turn fails to activate RhoA. Once the activity of Rac1 and RhoA diminishes, cells retract their membranes and grow processes. This model relies on the

Figure 8 (facing page). Ha-Ras-DN blocks bFGF-induced morphological changes but not Rac1-DN- or RhoA-DN-induced effects. (A–D) Images of cells infected with Ha-Ras-DN and left untreated (A and B) or treated with bFGF for 3 d (C and D). Infected cells were recognized by staining with an α-Ha-Ras mAb/FL conjugate (A and C), and the cells were identified as astrocytes by staining with α-GFAP/Cy-5 conjugate. (E and F) Ha-Ras-DN does not block the effects of Rac1-DN. Images of cells infected with Ad-Ha-Ras-DN plus Ad-Rac1-DN, grown for 2 d and stained with α-Ha-Ras/FL (E) together with α-Rac1/Cy5 (F). Note that although all cells are expressing the Ha-Ras-DN protein, only the process-bearing cell additionally expresses Rac1-DN. The α-Rac1 antibody used also recognizes antigenic sites in the nuclei of cells not infected with Ad-Rac1-DN. (G and H) Ha-Ras-DN does not block RhoA-DN-induced changes. Cells were infected with Ad-Ha-Ras-DN plus Ad-RhoA-DN, grown for 2 d, and stained with α-Ha-Ras/FL (G) together with α-RhoA/Cy5, which recognizes the RhoA-DN protein (H). Note that the process-bearing cells on the right express both Ha-Ras-DN and RhoA-DN. Bar, 27 μm.

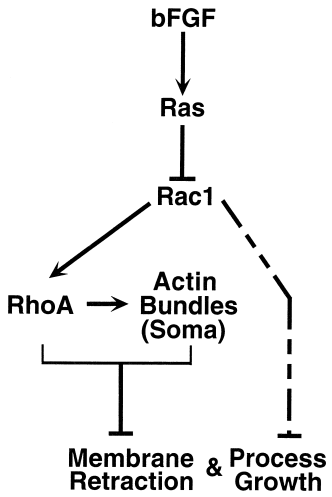

Figure 10. Model of bFGF signal transduction cascade in primary hippocampal CA1/CA3 astrocytes. In this model, Rac1 and RhoA are constitutively active in resting cells. Rac1 causes lamellipodia to form on the cell periphery, and RhoA maintains actin bundles. As in fibroblasts, Rac1 appears to act as an upstream activator of RhoA. Addition of bFGF activates Ha-Ras which in turn inhibits Rac1. Loss of Rac1 activity thereby results in loss of RhoA activity. This cascade leads to reorganization of actin bundles in the soma and membrane retraction. The cascade also causes initiation of process growth at discrete sites on the periphery. Although membrane retraction per se is independent of process growth, either RhoA or actin bundles or both inhibit process growth. Rac1 can directly affect process growth and membrane retraction (dashed line) in a manner that depends on the degree or site of inhibition or both.

assumption that the dominant negative alleles used here only directly affect the activity of endogenous GTPases of the same subtype and cannot exclude the possibility that blocking a downstream effector results in inappropriate or hyperactivity of upstream molecules, including other GTPases.

A Role for Ha-Ras in the bFGF Pathway

Our observation that Ha-Ras-DN blocks bFGF effects but not those of dominant negative Rac1 and RhoA suggests that bFGF activates Ha-Ras, which in turn inhibits Rac1 and RhoA; however, such a relationship between Ha-Ras and Rac1 is unusual. In fibroblasts, Ha-Ras has been reported to act, via PI-3 kinase (Rodriguez-Viciana *et al.*, 1997), as an upstream activator of Rac1 or RhoA (Ridley *et al.*, 1992).

Several factors might contribute to this difference. First, the phenotypes were observed on different time scales in the two systems (minutes to hours in the fibroblast system and days in the astrocyte system). With time scales on the order of days, transcriptional processes controlled by GTPases, or regulating their activity, could change the configuration of the cascade. Second, the two systems also differ with respect to the observed phenotypes (e.g., lamellipodia versus process growth) and it remains plausible that differently configured cascades control each. In addition, it is possible that differences in cell type can account for the apparent inconsistencies. In this regard, Cdc42 and/or Rac1 act in opposition to RhoA in developing growth cones of N1E-115 cells (Kozma *et al.*, 1997; Leeuwen *et al.*, 1997). Finally, we cannot rule out the possibility that the Ha-Ras-DN allele inhibits other Ras subtypes or otherwise acts nonspecifically. In this regard, biosafety considerations precluded generation of an adenovirus harboring the activated Ha-Ras allele.

Rac1 Activates RhoA in the bFGF Pathway

While both Rac1 and RhoA appear to be inhibited by bFGF, what is their relationship to one another? In fibroblasts, Rac1 is considered an upstream activator of RhoA, because Rac1* can produce not only lamellipodia but also stress fibers, and stress fiber production is blocked by RhoA-DN (Ridley and Hall, 1992; Nobes and Hall, 1995). RhoA* by contrast only produces stress fibers. We set out to order Rac1 and RhoA in astrocytes (Figure 7) by initiating process growth with Rac1-DN or Rho-DN and asking whether an activated allele of the opposite GTPase type could block. If Rac1 were upstream of RhoA as in the fibroblast system, then RhoA* would be expected to block Rac1-DN effects, and Rac1* would have no effect on Rho-A-DN effects.

Our observation that both combinations of GTPases blocked process growth and membrane retraction (Figure 7) did not at first appear to support an epistatic relationship reminiscent of that in the fibroblast system; however, closer examination of more subtle morphological changes such as actin and process shape revealed a pattern that was still consistent with Rac1 as an upstream activator of RhoA. In particular, actin bundles were restricted to the periphery of cells infected with Rac1* plus RhoA-DN (Figure 7, C and F). By contrast, actin appeared bundled throughout cells expressing Rac1-DN plus RhoA*, a pattern identical to that seen in untreated cells (Figure 2, A and B). We reasoned that were RhoA upstream of Rac1, bFGF treatment of Rac1*-infected cells would cause inhibition of endogenous RhoA and therefore recapitulate the conditions produced by coexpression of Rac1* and RhoA-DN; however, in bFGF-treated cells infected with Rac1*, actin appeared bundled throughout the cell and not restricted to the periphery (our unpublished results), a result consistent with Rac1 as an upstream activator of RhoA but not the other way around.

A model where Rac1 acts as an upstream activator of RhoA also accounts for other more subtle phenotypes. For example, the girth of RhoA-DN–induced processes appeared fivefold wider than that observed with bFGF or Rac1-DN. Such wide girths were not

evident in cells infected with RhoA-DN plus Rac1-DN (our unpublished results). Thus, the wider girth could result from high endogenous Rac1 activity causing lamellipodia to extend orthogonally along the length of each process. The effect of Rac1 on process girth described here may be similar to the wider girths apparent on processes of NGF-treated PC12 cells that overexpress Rac1* or PAK alleles (Daniels *et al.*, 1998). Finally, actin bundles were not evident in cells expressing Rac1-DN (Figure 3D), as expected if Rac1 acts upstream of RhoA.

Selective Inhibition of Rac1 Activity by bFGF

Some of our data support the possibility that bFGF regulates the extent to which Rac1 activity is inhibited or the cellular locale where inhibition occurs as a means of producing more subtle morphological phenotypes than process growth. For example, after bFGF treatment, lamellipodia appear on and along processes (Figure 2F). Lamellipodia in astrocytes, as in other systems, depend on endogenous Rac1 activity because none were evident in cells infected with Rac1-DN (Figure 3). Thus, while bFGF inhibits Rac1 activity enough to produce processes, it does not necessarily do so entirely or everywhere. The effects of bFGF stand in contrast to those of Rac1-DN, which when expressed throughout the cells produces processes without lamellipodia. The level of Rac1 activity may also affect the shape of processes. For example, RhoA-DN can still produce processes, albeit wider ones perhaps caused by unchecked levels of endogenous Rac1 activity, but overexpression of Rac1* precludes process growth under any conditions (e.g., in cells treated with bFGF or expressing RhoA-DN). Thus, bFGF may regulate the degree or locale of Rac1 activity or both to control not only whether processes form but also what shape they assume. We have indicated these locale- and activity-dependent effects of Rac1 on process growth in Figure 10 as an additional inhibitory pathway (dashed line). We speculate that molecules causing processes to form at distinct sites on the cell periphery, or causing actin to orient into growing processes, are negatively regulated by Rac1. bFGF might abrogate such inhibition, thereby allowing actin bundles polymerizing at distinct sites to cause membrane extrusion. bFGF also reorganizes actin in the soma by inhibiting Rac1 and RhoA to allow the membrane to retract. An important test of our model will be to measure the subcellular distribution of endogenous Rac1 and RhoA activity.

Process Growth in Neurons Versus Astrocytes: Cell Type–Specific Differences in GTPase Coupling

Several lines of evidence and data presented here suggest that the GTPase cascade controlling process growth is configured differently in neurons and astrocytes. In both neurons and astrocytes, RhoA appears to inhibit process growth (Figure 9E), whereas Rac1 activity appears inhibitory to astrocyte process growth (Figure 9C) but supports neuronal process growth (Figure 9D) (see also Kozma *et al.*, 1997; Leeuwen *et al.*, 1997), as well as the development of ancillary structures such as dendritic spines in vivo (Luo *et al.*, 1996). Moreover, Rac1 and RhoA activity do not appear to be coupled in neurons as they are in astrocytes and fibroblasts. Indeed, in the growth cone, these GTPases appear to antagonize one another (Kozma *et al.*, 1997; Leeuwen *et al.*, 1997). These differences in coupling may provide an explanation for why neurons, but not astrocytes, can regrow processes in culture. Thus, in neurons, culture conditions that activate Rac1 inhibit RhoA and support process growth, whereas in astrocytes, activating Rac1 and in turn RhoA inhibits process growth. We suggest that cell-type or locale-specific differences in the configuration of the cascade may be the rule rather than the exception when considering GTPase involvement in gross morphological changes such as process growth or even cell migration and scattering (Ridley *et al.*, 1995), activities that require complex cytoskeletal reorganization in different parts of the cell.

A GTPase Cascade Controls the Maintenance of Astrocyte Processes in Cultured Brain Tissue

Our results with the GTPases in organotypic slices (Figure 9) provide evidence that astrocytes in a more native setting than tissue culture must maintain Rac1 and RhoA activity at low levels to maintain their morphology. Although the relevance of these findings to astrocyte process growth in vivo remains uncertain, they do raise the testable possibility that the cascade we have defined here might apply in vivo. In this scenario, an as yet undetermined endogenous factor triggers the GTPase cascade. Several lines of evidence suggest that the signal derives from neurons. For example, neurons cause astrocyte process growth in vitro (Hatten, 1985; Gasser and Hatten, 1990), and astrocyte processes grow when electrical activity in neurons is blocked in vivo (Rubel and MacDonald, 1992). Although our results provide no evidence for a role for bFGF in vivo, it is a reasonable candidate. Astrocytes in the brain have FGF receptors (el-Husseini *et al.*, 1994; Morrison *et al.*, 1994; Gonzalez *et al.*, 1995) and both neurons and astrocytes synthesize FGF (Hatten *et al.*, 1988; Gonzalez *et al.*, 1995). Experiments with knockout mice have not yet defined a role for FGF receptor family members or ligands in astrocyte process growth, perhaps owing to functional redundancy among ligand and receptor family members or to early embryonic lethality (Arman *et al.*, 1998). Other growth factors must be considered candidates as well.

Several growth factors that have been reported to affect astrocyte morphology, including Bone Morphogenic Protein (Gross *et al.*, 1996), the cytokine interleukin 1β (Liu *et al.*, 1994), acidic FGF (Perraud *et al.*, 1988), and the neurotransmitter glutamate (Cornell-Bell *et al.*, 1990), are also likely candidates.

ACKNOWLEDGMENTS

We express our gratitude to the following investigators for gifts of reagents and use of equipment: Lisa Stowers and John Chant for PAK plasmids, Geoff Clark and Channing Der for RhoA plasmids, Michael Anderson for GFP plasmids, Tim Mitchison and members of his laboratory for use of microscopy equipment, Orion Weiner for help with deconvolution imaging, John Sedat for use of microscopy equipment, Lucy O'Brien for help with confocal imaging, Jack Parent and Anil Baghari for advice on organotypic cultures, and Christian Billante and Sue Giller for technical assistance. We thank Henry Bourne, Aneil Mallavarapu, Roger Nicoll, Lucy O'Brien, Louis Reichardt, and Ben Barres for commenting on an earlier version of this manuscript and for their helpful discussion. Yoram Altschuler, Keith Mostov, and Roger Nicoll provided invaluable advice and assistance. We also acknowledge Louise Cramer for her prescient advice at the outset of the project, and Aneil Malavarapu and Michael Anderson for their enlightening and invaluable discussion. S.N.G. was supported by a University of California at San Francisco Medical Scientist Training Program training grant (GM07618) and by an ARCS award. This work was supported by a grant from the National Cancer Institute (R35CA44338) to J.M.B.

REFERENCES

Arman, E., Haffner-Krausz, R., Chen, Y., Heath, J.K., and Lonai, P. (1998). Targeted disruption of fibroblast growth factor (FGF) receptor 2 suggests a role for FGF signaling in pregastrulation mammalian development. Proc. Natl. Acad. Sci. USA *95*, 5082–5087.

Baorto, D.M., Mellado, W., and Shelanski, M.L. (1992). Astrocyte process growth induction by actin breakdown. J. Cell Biol. *117*, 357–367.

Bignami, A., Eng, L.F., Dahl, D., and Uyeda, C.T. (1972). Localization of the glial fibrillary acidic protein in astrocytes by immunofluorescence. Brain Res. *43*, 429–435.

Cameron, R.S., and Rakic, P. (1991). Glial cell lineage in the cerebral cortex: a review and synthesis. Glia *4*, 124–137.

Chen, S.Y., Huff, S.Y., Lai, C.C., Der, C.J., and Powers, S. (1994). Ras-15A protein shares highly similar dominant-negative biological properties with Ras-17N and forms a stable, guanine-nucleotide resistant complex with CDC25 exchange factor. Oncogene *9*, 2691–2698.

Cornell-Bell, A.H., Thomas, P.G., and Smith, S.J. (1990). The excitatory neurotransmitter glutamate causes filopodia formation in cultured hippocampal astrocytes. Glia *3*, 322–334.

Cramer, L. (1997). Molecular mechanism of actin-dependent retrograde flow in lamellipodia of motile cells. Front. Biosci. *2*, 260–270.

Cramer, L., and Mitchison, T.J. (1993). Moving and stationary actin filaments are involved in spreading of postmitotic PtK2 cells. J. Cell Biol. *122*, 833–843.

Daniels, R.H., Hall, P.S., and Bokoch, G.M. (1998). Membrane targeting of p21-activated kinase 1 (PAK1) induces neurite outgrowth from PC12 cells. EMBO J. *17*, 754–764.

el-Husseini, A.e.-D., Paterson, J.A., and Shiu, R.P. (1994). Basic fibroblast growth factor (bFGF) and two of its receptors, FGFR1 and FGFR2: gene expression in the rat brain during postnatal development as determined by quantitative RT-PCR. Mol. Cell. Endocrinol. *104*, 191–200.

Ffrench-Constant, C., Miller, R.H., Kruse, J., Schachner, M., and Raff, M.C. (1986). Molecular specialization of astrocyte processes at nodes of Ranvier in rat optic nerve. J. Cell Biol. *102*, 844–852.

Gasser, U.E., and Hatten, M.E. (1990). Neuron-glia interactions of rat hippocampal cells in vitro: glial-guided neuronal migration and neuronal regulation of glial differentiation. J. Neurosci. *10*, 1276–1285.

Goldman, J.E., and Abramson, B. (1990). Cyclic AMP-induced shape changes of astrocytes are accompanied by rapid depolymerization of actin. Brain Res. *528*, 189–196.

Goldman, J.E., and Chiu, F.C. (1984). Growth kinetics, cell shape, and the cytoskeleton of primary astrocyte cultures. J. Neurochem. *42*, 175–184.

Gonzalez, A.M., Berry, M., Maher, P.A., Logan, A., and Baird, A. (1995). A comprehensive analysis of the distribution of FGF-2 and FGFR1 in the rat brain. Brain Res. *701*, 201–226.

Gossen, M., and Bujard, H. (1992). Tight control of gene expression in mammalian cells by tetracycline-responsive promoters. Proc. Natl. Acad. Sci. USA *89*, 5547–5551.

Gross, R.E., Mehler, M.F., Mabie, P.C., Zang, Z., Santschi, L., and Kessler, J.A. (1996). Bone morphogenetic proteins promote astroglial lineage commitment by mammalian subventricular zone progenitor cells. Neuron *17*, 595–606.

Hansson, E., and Ronnback, L. (1995). Astrocytes in glutamate neurotransmission. FASEB J. *9*, 343–350.

Hardy, S., Kitamura, M., Harris-Stansil, T., Dai, Y., and Phipps, M.L. (1997). Construction of adenovirus vectors through Cre-lox recombination. J. Virol. *71*, 1842–1849.

Hatten, M.E. (1985). Neuronal regulation of astroglial morphology and proliferation in vitro. J. Cell Biol. *100*, 384–396.

Hatten, M.E., Lynch, M., Rydel, R.E., Sanchez, J., Joseph-Silverstein, J., Moscatelli, D., and Rifkin, D.B. (1988). In vitro neurite extension by granule neurons is dependent upon astroglial-derived fibroblast growth factor. Dev. Biol. *125*, 280–289.

Khosravi-Far, R., Solski, P.A., Clark, G.J., Kinch, M.S., and Der, C.J. (1995). Activation of Rac1, RhoA, and mitogen-activated protein kinases is required for Ras transformation. Mol. Cell. Biol. *15*, 6443–6453.

Koyama, Y., and Baba, A. (1996). Endothelin-induced cytoskeletal actin reorganization in cultured astrocytes: inhibition by C3 ADP-ribosyltransferase. Glia *16*, 342–350.

Kozma, R., Ahmed, S., Best, A., and Lim, L. (1995). The Ras-related protein Cdc42Hs and bradykinin promote formation of peripheral actin microspikes and filopodia in Swiss 3T3 fibroblasts. Mol. Cell. Biol. *15*, 1942–1952.

Kozma, R., Sarner, S., Ahmed, S., and Lim, L. (1997). Rho family GTPases and neuronal growth cone remodelling: relationship between increased complexity induced by Cdc42Hs, Rac1, and acetylcholine and collapse induced by RhoA and lysophosphatidic acid. Mol. Cell. Biol. *17*, 1201–1211.

Leeuwen, F.N., Kain, F.E., Kammen, R.A., Michiels, F., Kranenburg, O.W., and Collard, J.G. (1997). The guanine nucleotide exchange factor Tiam1 affects neuronal morphology opposing roles for the small GTPases Rac and Rho. J. Cell Biol. *139*, 797–807.

Lester, R.A.I., Quarum, M.L., Parker, J.D., Weber, E., and Jahr, C.E. (1989). Interaction of 6-cyano-7-nitroquino-xaline-2,3-dione with the *N*-methyl-D-aspartate receptor-associated glycine binding site. Mol. Pharmacol. *35*, 565–570.

Liu, W., Shafit-Zagardo, B., Aquino, D.A., Zhao, M.L., Dickson, D.W., Brosnan, C.F., and Lee, S.C. (1994). Cytoskeletal alterations in human fetal astrocytes induced by interleukin-1 beta. J. Neurochem. *63*, 1625–1634.

Luo, L., Hensch,T.K., Ackerman, L., Barbel, S. Jan, L.Y., and Jan, L.N. (1996). Differential effects of the Rac GTPase on Purkinje cell axons and dendritic trunks and spines. Nature *379*, 837–840.

Mason, C.A., Edmondson, J.C., and Hatten, M.E. (1988). The extending astroglial process: development of glial cell shape, the growing tip, and interactions with neurons. J. Neurosci. *8*, 3124–3134.

Mennerick, S., Benz, A., and Zorumski, C.F. (1996). Components of glial responses to exogenous and synaptic glutamate in rat hippocampal microcultures. J. Neurosci. *16*, 55–64.

Mennerick, S., and Zorumski, C.F. (1994). Glial contributions to excitatory neurotransmission in cultured hippocampal cells. Nature *368*, 59–62.

Misson, J., Takahashi, T., and Caviness, V.S. (1991). Ontogeny of radial and other astroglial cells in murine cerebral cortex. Glia *4*, 138–148.

Morrison, R.S., Yamaguchi, F., Saya, H., Bruner, J.M., Yahanda, A.M., Donehower, L.A., and Berger, M. (1994). Basic fibroblast growth factor and fibroblast growth factor receptor I are implicated in the growth of human astrocytomas. J. Neurooncol. *18*, 207–216.

Neering, S.J., Hardy, S.F., Minamoto, D., Spratt, S.K., and Jordan, C.T. (1996). Transduction of primitive human hematopoietic cells with recombinant adenovirus vectors. Blood *88*, 1147–1155.

Nobes, C.D., and Hall, A. (1995). Rho, rac, and cdc42 GTPases regulate the assembly of multimolecular focal complexes associated with actin stress fibers, lamellipodia, and filopodia. Cell *81*, 53–62.

Peppelenbosch, M.P., Qiu, R.G., de Vries-Smits, A.M., Tertoolen, L.G., de Laat, S.W., McCormick, F., Hall, A., Symons, M.H., and Bos, J.L. (1995). Rac mediates growth factor-induced arachidonic acid release. Cell *81*, 849–856.

Perraud, F., Besnard, F., Pettmann, B., Sensenbrenner, M., Labordette, G. (1988). Effects of acidic and basic fibroblast growth factors (aFGF and bFGF) on the proliferation and the glutamine synthetase expression of rat astroblasts in culture. Glia *1*, 124–131.

Ramsay, G., Evan, G.I., and Bishop, J.M. (1984). The protein encoded by the human proto-oncogene c-myc. Proc. Natl. Acad. Sci. USA *81*, 7742–7746.

Ridley, A.J., Comoglio, P.M., and Hall, A. (1995). Regulation of scatter factor/hepatocyte growth factor responses by Ras, Rac, and Rho in MDCK cells. Mol. Cell. Biol. *15*, 1110–1122.

Ridley, A.J., and Hall, A. (1992). The small GTP-binding protein rho regulates the assembly of focal adhesions and actin stress fibers in response to growth factors. Cell *70*, 389–399.

Ridley, A.J., Paterson, H.F., Johnston, C.L., Diekmann, D., and Hall, A. (1992). The small GTP-binding protein rac regulates growth factor-induced membrane ruffling. Cell *70*, 401–410.

Rodriguez-Viciana, P., Warne, P.H., Khwaja, A., Marte, B.M., Pappin, D., Das, P., Waterfield, M.D., Ridley, A., and Downward, J. (1997). Role of phosphoinositide 3-OH kinase in cell transformation and control of the actin cytoskeleton by Ras. Cell *89*, 457–467.

Rubel, E.W, and MacDonald, G.H. (1992). Rapid growth of astrocytic processes in N. magnocellularis following cochlea removal. J. Comp. Neurol. *318*, 415–425.

Sontheimer, H. (1995). Glial neuronal interactions: a physiological perspective. Neuroscientist *1*, 328–337.

Stoppini, L., Budas, P.A., and Muller, D. (1991). A simple method for organotypic cultures of nervous system. J. Neurosci. Methods *37*, 173–182.

Threadgill, R., Bobb, K., Ghosh, A. (1997). Regulation of dendritic growth and remodeling by Rho, Rac, and Cdc42. Neuron *19*, 625–634.

Van Aelst, L., and D'Souza-Schorey, C. (1997). Rho GTPases and signaling networks. Genes Dev. *11*, 2295–2322.